Indian Journal of Radio & Space Physics
Vol. 35, June 2006, pp. 206-211

Theoretical and experimental investigations of circular sector microstrip antenna

Vijay Kumar Tiwari, Aradhana Kimothi, D Bhatnagar, J S Saini & V K Saxena
Microwave Lab., Department of Physics, University of Rajasthan, Jaipur 302 004, India
and
P Kumar
Communication System Group, ISRO Satellite Centre, Banglore 560 017, India

Received 20 May 2005; accepted 25 November 2005

An analysis of a general circular sector microstrip antenna (CSMA) with sector angle, α, is presented in this paper. The theoretical analysis is carried out by applying cavity model-based modal expansion technique. The computed results are validated with measured results for CSMA geometry with $\alpha = 60^{o}$. The computed results show a fairly good agreement with measured results. A reasonably small deviation of 1.06% in the resonant frequency is recorded, while a fairly good agreement between measured and computed return loss and radiation patterns is recorded. This validates the proposed technique of treating CSMA geometry.

Keywords: Microstrip antennas, Cavity model, Radiation patterns, Input impedance
PACS No.: 84.40.Ba, 75.50.Gg
IPC Code: H01Q9/00; H01Q21/00; H01Q23/00

1 Introduction

Circular and rectangular geometries of microstrip antennas are most popular among the scientific community due to different reasons. However, geometrical constraints become vital when radiators are needed for conformal mounting on pre-existing structures. Under this condition, other shapes of antennas as per geometry of host structure should be used. In recent years, Sultan[1,2] analyzed gap, open ring and annular sector antennas. Guo *et al.*[3] analyzed an annular ring antenna and Wong[4] investigated a ring slot antenna to search the possibilities of replacing rectangular and circular microstrip antenna geometries with these geometries. Microstrip antennas, in general, have inherent narrow bandwidth and low gain. Therefore, these antennas, in general, found very limited application in different fields. Looking their compactness, these antennas are now found more suitable for mobile applications and hence serious efforts started to remove their inherent drawbacks.

2 Antenna geometry and theoretical formulation

The mode dependent theoretical study on the radiation properties of circular sector microstrip antennas (CSMA) having sector angle, α, is carried out. The CSMA with coordinate system is shown in Fig. 1. It consists of a planer circular sector of sector angle α, radius a, on a thin dielectric substrate of thickness h ($h<<\lambda_0$), relative substrate permittivity ε_r and loss tangent tan(δ). The z-axis is perpendicular to the plane of the patch. The theoretical analysis of proposed geometry is carried out by applying cavity model-based modal expansion technique[5], because it requires less computational efforts but provides good compromise between complexity of modes and accuracy of results.

The region between the patch and ground plane is treated as a cavity bounded by a magnetic wall along the edge of the patch and electric walls above and below. The electric field has only the z component, while magnetic field has transverse components in the region bounded by the conducting patch and the ground plane. The modelling of coaxial feed is done by assuming a current ribbon of effective thickness $2w$, centred on the feed axis at a distance d from the centre of the patch. The patch is excited in such a way that the input filamentary current[6] at feed location (d, φ'') is

$$J = J_z(\varphi')\frac{\delta(\rho - d)}{d}\hat{z} \qquad \ldots(1)$$

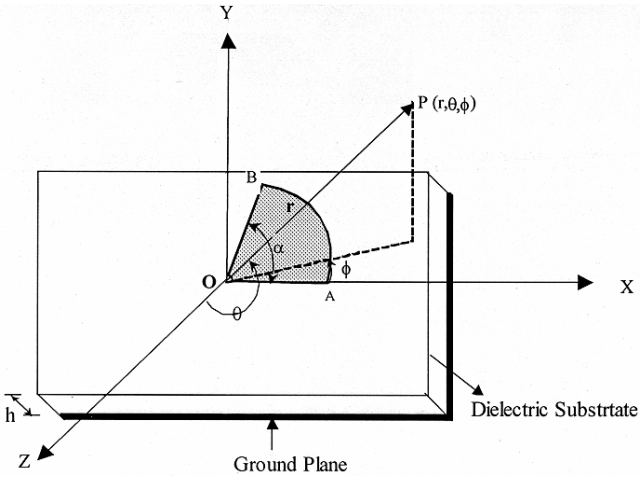

Fig. 1—Geometry and co-ordinate system of circular sector microstrip antenna (CSMA)

with

$$J_z(\varphi') = J, \quad \varphi'' - w < \varphi' < \varphi'' + w$$
$$= 0, \quad \text{elsewhere}$$

The electric field produced by this filamentary unit electric current source is given by

$$E_z = E_0 J_\nu\left(K_{\nu m}\rho\right)\cos(\nu\varphi') \qquad \ldots(2)$$

with

$$E_0 = -j\omega\mu \sum\sum \frac{2\,\frac{\sin(\nu w)}{\nu}\cos(\nu\varphi'')J_\nu(K_{\nu m}d)}{(K^2 - K_{\nu m}{}^2)\frac{1}{4}\left[J_\nu\left(K_{\nu m}a\right)\right]^2} \times\left[a^2 - \frac{\nu^2}{K_{\nu m}^2}\right]\left[\alpha + \frac{\sin(2\nu\alpha)}{2\nu}\right] \qquad \ldots(3)$$

Here, $K_{\nu m}$ is the resonant wave number, $K = k_0\sqrt{\varepsilon_r\left(1 - j\tan(\delta)\right)}$ the wave number of the dielectric substrate used for antenna, $J_\nu\ (K_{\nu m}\ a)$ the cylindrical function of first kind of Bessel function of order ν, and

$$\nu = n, \quad if \qquad \alpha = 2\pi$$
$$= \frac{n\pi}{\alpha}, \quad \text{othewise} \qquad \ldots(4)$$

Resonance occurs when $K = K_{\nu m} = \chi_{\nu m}/a$

Here, $\chi_{\nu m}$ is the m^{th} zero of the function $J_\nu'\ (K_{\nu m}a)$.

3 Resonance frequency

The resonance frequency of CSMA geometry in TM_{nm} mode is calculated analytically by applying

$$f_r = \frac{\left(K_{\nu m}a\right)c}{2\pi a_e\sqrt{\varepsilon_d}} \qquad \ldots(5)$$

Here, a_e is the effective radius of the patch, ε_d is the dynamic permittivity which is a function of dimensions of patch, equivalent permittivity of substrate material and field distribution under the patch for the mode under consideration and is given by[7]

$$\varepsilon_d = C_d(\varepsilon)/C_d(\varepsilon_0) \qquad \ldots(6)$$

where $C_d(\varepsilon)$ is the total dynamic capacitance defined as

$$C_d(\varepsilon) = C_{0,d} + C_{e,d} \qquad \ldots(7)$$

where $C_{0,d}$ and $C_{e,d}$ are the dynamic main and fringing capacitance, respectively and $C_d(\varepsilon_0)$ is the total dynamic capacitance when $\varepsilon = \varepsilon_0$.

The dynamic main capacitance $C_{0,d}$ for a circular disk microstrip antenna given by Wolff and Knoppik[8] is modified for a circular sector antenna by incorporating patch area in the expression, i.e.

$$C_{0,d} = \frac{\varepsilon\alpha a^2}{2h\delta}\left[1 - \frac{J_{\nu-1}(K_{\nu m}\,a)J_{\nu+1}(K_{\nu m}\,a)}{J^2{}_\nu(K_{\nu m}\,a)}\right] \qquad \ldots(8)$$

with

$$\delta = 1 \quad \text{for } n = 0$$
$$= 2 \quad \text{for } n \neq 0$$

The dynamic fringe field capacitance $C_{e,d}$ is calculated by replacing the circular sector patch by a circular patch of radius r having an equivalent surface area[9]. The radius of this circular patch is

$$r = a\sqrt{\frac{\alpha}{2\pi}} \qquad \ldots(9)$$

The expression of dynamic fringing capacitance $C_{e,d}$ given in Ref. 8 is also modified for the circular sector antenna, i.e.

$$C_{e,d} = \frac{1}{\alpha}\int_0^{\alpha} C_{e,s}(\varepsilon)\cos^2(\nu\varphi)\,d\varphi \qquad \ldots(10)$$

Here, $C_{e,s}$ represents the static fringing capacitance of the dominant mode due to the fringing fields at the edge as defined in Ref.7. The modified expression of $C_{e,s}$ for the present geometry will be

$$C_{e,s} = \frac{\varepsilon\alpha a^2}{2h}\left[\left(1+\frac{2h}{\pi\varepsilon_r r}\ln\left(\frac{r}{2h}\right)+(1.41\varepsilon_r+1.77)\right)+\frac{h}{r}(0.268\varepsilon_r+1.65\right] \qquad \ldots(11)$$

In the same way, $C_d(\varepsilon_0)$ can also be obtained by replacing ε by ε_0 in above formulas.

The fringing field effects are included by introducing effective patch radius a_e in Eq. (5) which is calculated by using radius extension expression of the circular patch having the same surface area as that of circular sector patch and is given by

$$a_e = r_e\sqrt{\frac{2\pi}{\alpha}} \qquad \ldots(12)$$

where r_e represents the effective radius of the circular patch given by[9]

$$r_e = r\left[1+\frac{2h}{\pi\varepsilon_r r}\left(\ln\left(\frac{r}{2h}\right)+(1.41\varepsilon_r+1.77)+\frac{h}{r}(0.268\varepsilon_r+1.65\right)\right]^{\frac{1}{2}} \qquad \ldots(13)$$

On substituting $\alpha = 2\pi$ and $\nu = n$, all the above relations convert into those for a circular patch microstrip antenna. The computed and simulated resonance frequencies for different antenna structures in dominant mode of excitation are given in Table 1. A fairly good agreement between computed and simulated resonant frequency is obtained that validates above formulations of resonant frequency.

4 Far-field components and radiation pattern factor

By applying equivalence principle and image theory, components of equivalent magnetic current sources $\vec{\mathbf{M}}$, i.e. M_φ which represents outer M source associated with curved edge and equivalent source associated linear edges ($M_{\rho 1}$) and ($M_{\rho 2}$) are calculated, i.e.

$$M_\varphi = 2E_0 J_\nu\left(K_{\nu m}a\right)\cos\left(\nu\varphi'\right) \qquad \ldots(14)$$

$$M_{\rho 1} = 2E_0 J_\nu\left(K_{\nu m}a\right)\cos\left(\nu 0\right) \qquad \ldots(15)$$

$$M_{\rho 2} = 2E_0 J_\nu\left(K_{\nu m}a\right)\cos\left(\nu\alpha\right) \qquad \ldots(16)$$

These expressions are then applied to compute different components of vector potential $\vec{\mathbf{F}}$ in the cylindrical coordinate system, i.e.

$$F_{\varphi'} = \frac{\varepsilon_0}{4\pi}h\,a_e\int_0^{\alpha} M_\varphi\, e^{jk_0 a_e\sin\theta.\cos(\varphi'-\varphi)}\,d\varphi' \qquad \ldots(17)$$

For straight edge OA shown in Fig.1, $\varphi' = 0$.

$$F_{\rho 1} = \frac{\varepsilon_0}{4\pi}h\int_0^{a_e} M_{\rho 1}\, e^{jk_0 a_e\sin\theta.\cos(\varphi'-\varphi)}\,d\rho \qquad \ldots(18)$$

and for straight edge OB, $\varphi' = \alpha$

$$F_{\rho 2} = \frac{\varepsilon_0}{4\pi}h\int_{a_e}^{0} M_{\rho 2}\, e^{jk_0 a_e\sin\theta.\cos(\varphi'-\varphi)}\,d\rho \qquad \ldots(19)$$

Table 1—Computed and simulated resonance frequency of some antenna geometries (h =1.59 mm)

Geometry	Patch radius (a) mm	Substrate permittivity (ε_r)	Resonance frequency, GHz	
			Calculated	Simulated with IE3D software
Circular sector (α=60°)	30	2.55	3.958	3.96
Circular sector (α=90°)	30	2.55	2.90	2.94
Semi circular patch (α=180°)	20	2.32	2.814	2.810
Circular sector (α=355°)	20	2.55	2.647	2.65
Circular patch (α=360°)	16.64	3.55	2.700	2.700

By applying suitable transformations, the expressions of far zone electric field factor R_{th} of the proposed geometry is obtained in terms of F_ρ and $F_{\varphi'}$ as:

$$E_\theta = -j\omega\eta_0 \left[F_\rho \sin(\varphi' - \varphi) + F_{\phi'} \cos(\varphi' - \varphi) \right] \quad \ldots(20)$$

$$E_\varphi = +j\omega\eta_0 \begin{bmatrix} F_\rho \cos(\theta)\cos(\varphi' - \varphi) \\ -F_{\phi'} \cos(\theta)\sin(\varphi' - \varphi) \end{bmatrix} \quad \ldots(21)$$

The total field pattern factor of antenna in free space is obtained by using the relation

$$R_{th} = \left[|E_\theta|^2 + |E_\varphi|^2 \right] \quad \ldots(22)$$

The frequency dependent input impedance of probe-fed CSMA geometry is determined using the following relation

$$Z_{in} = V_{in} / I_0 \quad \ldots(23)$$

Here, the RF voltage V_{in} at the feed point is calculated from the average electric field as

$$V_{in} = \frac{-h}{2w} \left[\int_{\varphi^* - w}^{\varphi^* + w} E_z(d, \varphi)\, d\varphi \right] \quad \ldots(24)$$

and the feed current is

$$I_0 = 2 J w \quad \ldots(25)$$

On simplifying above relations, the following expression for input impedance of CSMA geometry is obtained:

$$Z_{in} = j\omega\mu \sum\sum \frac{2J \left(\frac{\sin(v w)}{v w} \right)^2 \cos(v\varphi'') \left(J_v(K_{vm} d) \right)^2}{(K^2(1 - j\delta_{eff}) - K_{vm}^2) \frac{1}{4} \left[J_v(K_{vm} a) \right]^2} \times \left[a^2 - \frac{v^2}{K_{vm}^2} \right] \left[\alpha + \frac{\sin(2v\alpha)}{2v} \right] \quad \ldots(26)$$

Here, δ_{eff} is the effective value of loss tangent and taken equal to $\frac{1}{Q_t}$, where Q_t is the total quality factor that involves all the losses associated with a microstrip patch antenna. Once input impedance of antenna is known, return loss values may be obtained easily.

5 Experimental details

Geometry of a CSMA as shown in Fig. 2, is fabricated on Teflon fiber glass (TFG) substrate for experimentation. The sector angle (α) of designed antenna is 60°, patch radius (a) is 3.0 cm; substrate thickness (h) is 0.159 cm; substrate relative permittivity (ε_r) is 2.55; thickness of conducting copper with Sn-Pb coating is 35 μm and dimensions of ground plane are 7.5 cm × 6.5 cm. The patch is coaxially fed with a SMA connector. The feed location *(d, φ″)* of designed antenna is kept (13.75 mm, 0) as shown in Fig. (2).

The radiation patterns of designed antenna are measured at Indian Space Application Centre (ISAC), Bangalore. Both designed antenna and receiving standard horn antenna are kept around two metres apart inside an anechoic chamber. With a sweep generator, 3.916 GHz signal is applied and radiation patterns of test antenna are measured in φ = 0 and φ = 90° planes. The return loss and input impedance of designed antenna are measured with HP vector network analyzer and its associated computer programmes. Due consideration is given during impedance measurement to accuracy enhancement techniques to correct effective directivity, effective source match and frequency tracking errors.

6 Comparison of theory with experiment

The validity and accuracy of proposed method is first verified by comparing computed return loss results with simulation results obtained with IE3D simulation software. The feed location *(d, φ″)* is kept identical, i.e. (13.75 mm, 0) in both these conditions. These variations are shown in Fig. 3. A small

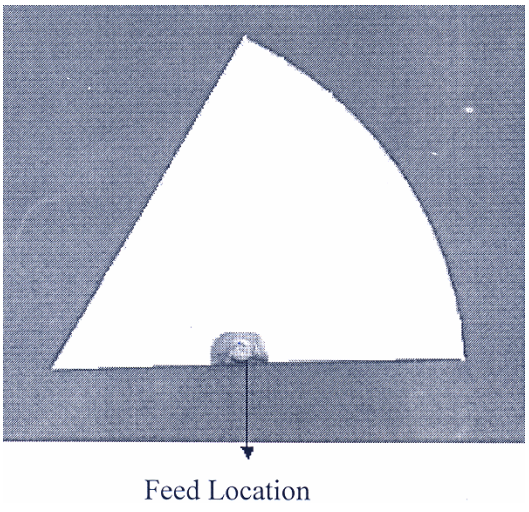

Fig. 2—Designed antenna for experimentation

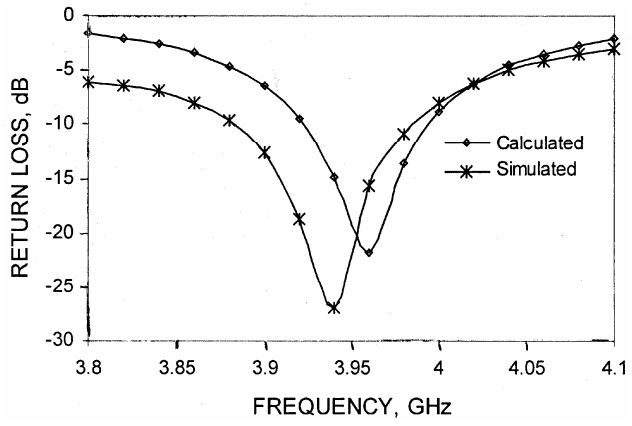

Fig. 3–Comparison between computed and simulated return loss of CSMA

Table 2—Computed and measured resonance frequency of circular disk microstrip antenna in TM_{11} mode of excitation (ε_r = 2.65, h =1.5875 mm)

Patch radius (a), mm	Calculated resonance frequency, GHz	Measured resonance frequency[10], GHz
11.5	4.415	4.425
10.7	4.724	4.723
9.6	5.228	5.224
8.2	6.049	6.074
7.4	6.646	6.634

Table 3—Computed and measured resonance frequency of circular disk microstrip antenna in different modes of excitation (a = 50 mm, ε_r = 2.32, h =1.59 mm)

Mode of excitation	Calculated resonance frequency, MHz	Measured resonance frequency[11], MHz
TM_{11}	1133	1128
TM_{21}	1882	1879
TM_{31}	2591	2596

difference of 18 MHz, i.e. 0.45% between computed and simulated frequency is recorded. Another comparison may be seen in Tables 2 and 3 where computed resonance frequency of CSMA geometry with α = 360° is compared with available measured results[10,11]. An excellent agreement between computed and measured resonance frequencies in different modes of excitation is again recorded. This validates the accuracy of present formulation.

After these remarkable agreements, a CSMA structure with α = 60° was designed keeping feed location again (13.75mm, 0) and its return loss was measured. As shown in Fig. 4, the dominant mode measured return loss of this antenna at resonance frequency is 5.74 dB larger than the computed value of return loss. However, a small difference of 1.06%

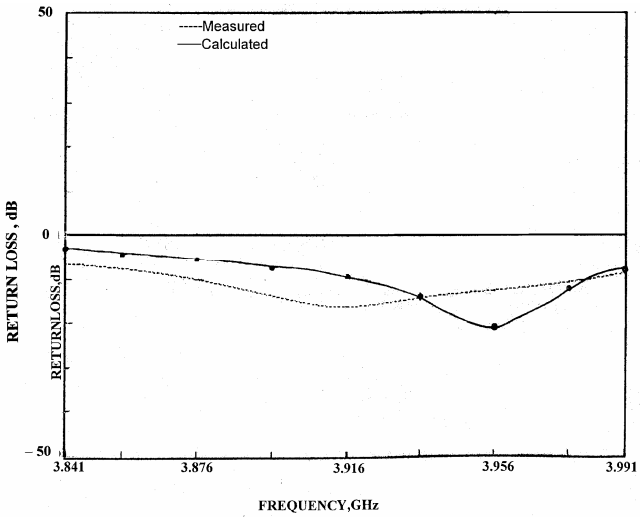

Fig. 4—Measured and computed return loss of antenna under test

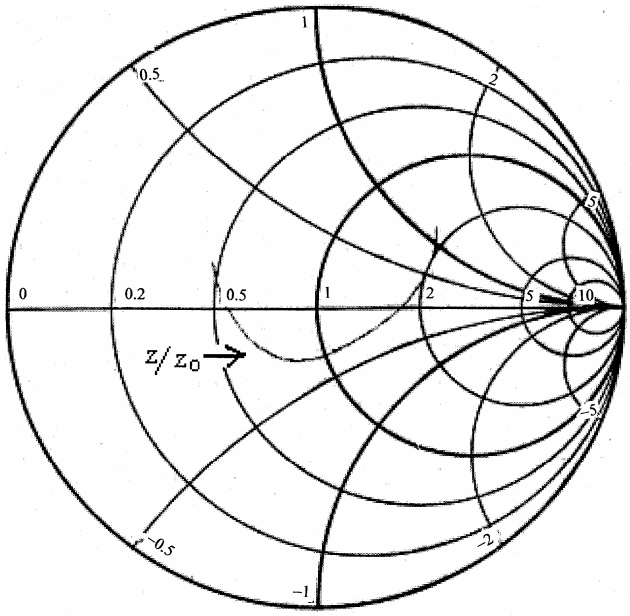

Fig. 5—Measured input impedance of antenna under test

between computed and measured resonance frequencies is recorded. A representative plot for measured input impedance of designed antenna is shown in Fig. 5. The frequency is changed from 3.841 GHz to 3.991 GHz in the steps of 0.2 GHz. The graph is plotted on the reduced scale and the total span of the variation in frequency is 150 MHz, i.e. 75 MHz on each side of resonance frequency. The measured input impedance of antenna at resonance frequency is 43.25 – j10.92, which is lower than the desired impedance of 50.35 + j7.0 ohm that we obtained by using Eq. (26). The measured bandwidth of antenna at resonance frequency is 1.53%, which is little lower

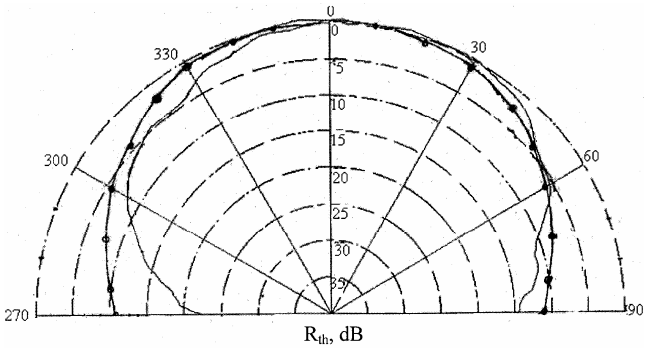

Fig. 6—Measured and computed *E*-plane radiation patterns

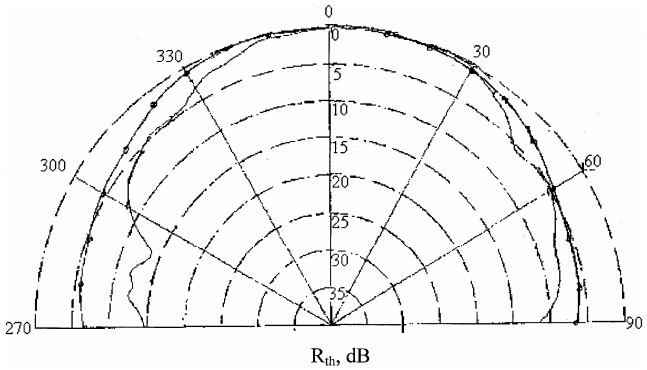

Fig. 7—Measured and computed *H*-plane radiation patterns

than the calculated bandwidth (1.08%) of this antenna.

The measured and computed *E* ($\varphi = 0$) and *H* ($\varphi = \pi/2$) plane normalized radiation patterns of CSMA geometry with $\alpha = 60°$ are shown in Figs 6 and 7, respectively. A relatively good agreement of shapes and 3 dB beamwidth of computed and measured patterns is recorded. Maximum radiations are in the broadside direction. The theoretical patterns are drawn by applying Eqs (20)-(22). A little discrepancy in these plotted patterns is due to inaccuracies of experimental measurements owing to the finite size of the ground plane. Further, during theoretical formulation, several simplifying assumptions are made which are necessary to make formulation easy.

7 Conclusions

The proposed technique is capable in predicting the resonance frequency of any circular sector microstrip antenna with greater accuracy. Due consideration is given to modal effects by evaluating dynamic permittivity in place of traditionally applied effective permittivity of substrate material. The fringe field effects, radiation losses, conductor losses and dielectric losses are also included in the computation. The theory is verified with measured results and a fairly good agreement in resonance frequency, return loss and radiation patterns is obtained.

Acknowledgements

The authors are thankful to Dr S Pal, Dr Lakshmeesha from ISAC, Bangalore, for granting permission for simulation work and experimentation at their centre. One of the authors (VKT) is thankful to CSIR, New Delhi, for providing him the research fellowship.

References

1 Sultan M A, The Mode Features of an Ideal-Gap Open Ring Microstrip Antenna, *IEEE Trans Antennas & Propag (USA), AP*-37 (1989) 137.

2 Sultan M A & Tripathi V K, The Mode Features of an Annular Sector Microstrip Antenna, *IEEE Trans Antennas & Propag (USA), AP*- 38 (1990) 265.

3 Guo Y X, Luk K M & Lee K F, L-Probe Proximity-Fed Annular Ring Microstrip Antennas, *IEEE Trans Antennas & Propag (USA), AP*-49 (2001) 19.

4 Wong L K, Haung C C & Chen W S, Printed Ring Slot Antenna for Circular Polarization, *IEEE Trans Antennas & Propag (USA), AP*-50 (2002) 75.

5 Carver K R & Mink J W, Microstrip Antenna Technology, *IEEE Trans Antennas & Propag (USA), AP*-29 (1981) 2.

6 Lo Y T, Solomon D & Richards W F, Theory and Experiment on Microstrip Antenna, *IEEE Trans Antennas & Propag, (USA), AP*-27 (1979) 137.

7 Abboud F, Damiano J P & Papiernik A, A New Model for Calculating the Input Impedance of Coax-Fed Circular Microstrip Antenna with and without Air Gaps, *IEEE Trans Antennas & Propag (USA), AP*-38 (1990) 1882.

8 Wolff I & Knoppik N, Rectangular and Circular Microstrip Disk Capacitors and Resonators, *IEEE Trans Microw Theory & Tech (USA)*, *AP*-22 (1974) 857.

9 Gurel C S & Yazgan E, New Computation of the Resonant Frequency of a Tunable Equilateral Triangular Microstrip Patch, *IEEE Trans Microw Theory & Tech (USA)*, 48 (2000) 334.

10 Itoh T & Mittra R, Analysis of Microstrip Disk Resonator, *Arch Eleck Ubertrag (Germany)*, 27 (1973) 456.

11 Dahele S, Mem S & Lee K F, Theory and Experiment on Microstrip Antenna with Air Gaps, *Proc Inst Elect Eng, Pt-H* (*UK*), 132 (1985) 455.